Heliyon 6 (2020) e05626

Contents lists available at ScienceDirect

Heliyon

journal homepage: www.cell.com/heliyon

Research article

Geotechnical evaluation of clayey materials for quality burnt bricks

George Oluwole Akintola *, Francis Amponsah-Dacosta, Sphiwe Emmanuel Mhlongo

Department of Mining and Environmental Geology, School of Environmental Sciences, University of Venda, Thohoyandou 0950 Limpopo, South Africa

ARTICLE INFO

Keywords:
Geochemistry
Geology
Materials science
Civil engineering
Geotechnical evaluation
Clayey material
Kaolinite-rich clay
Chlorite-rich clay
Burnt brick

ABSTRACT

Understanding of clayey materials properties continues to elude brick manufacturers, hence unsure of their application for brick making purposes. The raw materials were assessed geochemically, mineralogically, physically and technologically. The geochemical result showed that the fluxing oxides K_2O, N_2O, CaO, MgO and MnO are generally low in content with average abundance ranging from 0.06% to 1.78%. The Fe_2O_3 content varies (4.8–25.5%) thus reflects heterogenous stability in tonality. Most of the studied samples have relatively high Al_2O_3 content which suggest the bauxitic composition from which kaolinite minerals might have resulted from. The XRD analysis revealed the presence of kaolinite and chlorite as the major clay minerals while quartz, feldspar, talc and hornblende were present as non-clay minerals. For DTA, the threshold of new crystallization processes were attained at 1000 °C. The SEM analysis revealed the presence of some stroma in all samples although with sizes >50 nm. These pores were suggested to constitute a capillary system where molten mineral occupy as temperature increases. The Atterberg's limit indicated that the studied materials are inorganic silts with high compressibility and organic clays properties since it plotted below the A-line of plasticity chart. The compressive strength (CS) for brick specimens made from kaolinite-rich material are relatively higher than chlorite-rich specimens. This was attributed to the ineffective pore connection within the kaolinite interstitial particles compared to the chlorite-rich specimen, hence increasing the density. The water absorption (WA) test on twenty brick specimens showed that the pore volume and capillarity for bricks which are chlorite-dominated were comparatively higher, thus absorbing more water molecules. These results revealed that majority of the studied clayey material are not suitable for double storey construction bricks but meet the requirements for single-storey construction when compared with SANS standards.

1. Introduction

The demand of clayey material for different purposes is acknowledged in different parts of the world due to its ubiquitous distribution. As the interest in commercial application of clayey material for construction purposes is increasing owing to globalization and urbanization, Lahcen et al. (2014) emphasized the importance of proximity to construction sites since clayey materials have low unit value. Apparently, transportation of raw clay materials, proximity to beneficiating point, human resources, power and amenities strongly influence the mining of clayey deposits (Seong, 2005). Meanwhile, clayey materials differ in properties from region to region because their physical, chemical, mineralogical and mechanical properties are specific to various rock type distribution, diagenetic and weathering processes that contributed to their deposition (Lahcen et al., 2014; Manoharan et al., 2012). Clayey materials rich in iron content and lack of fluxing oxides have been suggested to exhibit poor mechanical resistance to compressive test thus not suitable as masonry units (Mahmoudi et al., 2008). Mechanical resistance and durability of burnt brick are considered to improve as thermal conductivity, strength and fluxing materials increases while the water absorption rate remains minimal (Ntouala et al., 2016; Fadil-Djenabou et al., 2015).

In the Thulamela region of South Africa, rise in demand for clayey materials has been driven primarily by increase in construction and civil activities due to urbanization and infrastructural development (Dacosta et al., 2013). This demand cannot be met with the traditional methods of brick manufacturing hence the need to characterize and evaluate the materials for masonry units. Meanwhile, many research have assessed the use of clayey materials for final brick products but their findings cannot be implemented at other regions due to their heterogenous distribution (Fadil-Djenabou et al., 2015; Boussen et al., 2016; Mahmoudi et al., 2017; El Idrissi et al., 2018). The empirical assessment of clayey material employs the use of suitability diagram such as Winkler's to suggest application for common bricks, vertically perforated bricks,

* Corresponding author.
E-mail address: georgeakintola540@gmail.com (G.O. Akintola).

https://doi.org/10.1016/j.heliyon.2020.e05626
Received 28 November 2019; Received in revised form 20 March 2020; Accepted 25 November 2020

hollow products and roofing tiles and masonry bricks (Yongue-Fouateu et al., 2016; Loutou et al., 2019). On the other hand, technological evaluation provides the practical and technical use of the final clay product by comparing the brick's strength and water absorption capacity with the requirements of regulatory organizations such as South Africa National Standard (SANS) and American Society for Testing and Material (ASTM). To date, no technological evaluation of clayey materials for burnt brick making has been reported in Thulamela regions despite several work on clayey materials (Murray, 2000; Hajjaji et al., 2002; Ekosse, 2010; Diko et al., 2011; Manoharan et al., 2012; Obaje et al., 2013; Dacosta et al., 2013; Refaey et al., 2015; Boussen et al., 2016; El Idrissi et al., 2018). However, the heterogeneous nature clay material invalidates the generalization of its application for burnt bricks due to varying nature of bedrock, regional topographic and climatic condition. To resolve this problem, the study aims to characterize and technically evaluate the Thulamela clayey materials for brick making purposes.

2. Study area

The Thulamela municipality area from which samples were collected is situated between latitude $22^0 15' 00'' S$ and $22^0 30' 00'' S$ longitude $30^0 09' 00'' E$ and $31^0 00' 56'' E$ (Figure 1). The sediment thickness varies at different locations and has an estimated thickness of 200 m in the Mutshindudi Natal House agglomerate north of Thohoyandou but best developed in the Kruger National Park (Barker et al., 2006). The area is geologically characterized with pyroclastic lava of about 3000 m thickness which intercalates sedimentary rock with tuffaceous rock (Bordy and Catuneanu, 2002). Stratigraphically, the study area, Thulamela Municipality, falls within the geology of Soutpansberg Group of Sedimentary and Volcanic rocks (Anhaeusser, 2006). It represents a volcano-sedimentary succession in chronological order of Tshifhufhu, Sibasa, Fundudzi, Wyllie's Poort, Nzhelele, Stayt and Mabiligwe Formations (Barker et al., 2006). However, Thulamela Municipality is dominantly underlain by the Sibasa Formation which comprises mainly of arenaceous and argillaceous rocks with a few thin pyroclastic beds (Barker et al., 2006). Retrospective studies (Kroner et al., 1999, 2000, Xie et al., 2017) have indicated that the clayey argillaceous formations, with estimated thickness of 1900 m, constituted great economic deposits for traditional pottery maker in a non-mechanized way.

3. Materials and methods

3.1. Sampling

The clayey raw materials were obtained from soils derived from basaltic rock which widely underlain the study area. Based on texture and colour variation, a total of fifteen clayey soil samples were collected from five different locations designated L1 to L5 coded as Lwa, Nan, Mat, Mav and Man respectively after the locality or village names. The samples were randomly collected from each location and thoroughly mixed until homogeneity was achieved and then quartered into five representative samples. The representative samples which correspond to each location were finally analyzed in the laboratory for various characterizations while brick specimen briquettes were molded as well for technological test.

3.2. Mineralogical analysis

Mineralogical composition of fine powders of the bulk fractions were semi-quantitatively determined using X-ray Diffraction (XRD) analysis at the University of Pretoria Lab. The bulk mineralogy of sediments was analysed at 15 cm intervals, depending on changes in sedimentary facies and colours (Jung et al., 2019). The fine clay fraction samples were dispersed in 0.7 mg/mL of distilled water and put in an ultrasonic water bath for 40 s to prevent flocculation of particles (Jung et al., 2019). Then, air-dried samples were made by pipetting sediment dispersions onto slide glasses for XRD analysis. After glycolation and oven-drying the samples at 300 °C for 1 h, sample was tightly mounted on oriented sample holder with very little pressure using black loading preparation technique for XRD analysis. The analysis was performed using PANalytical X'Pert Pro powder diffractometer equipped with X'Celerator detector coupled with receiving slits, variable divergence and Fe-filtered Cu-Kα radiation.

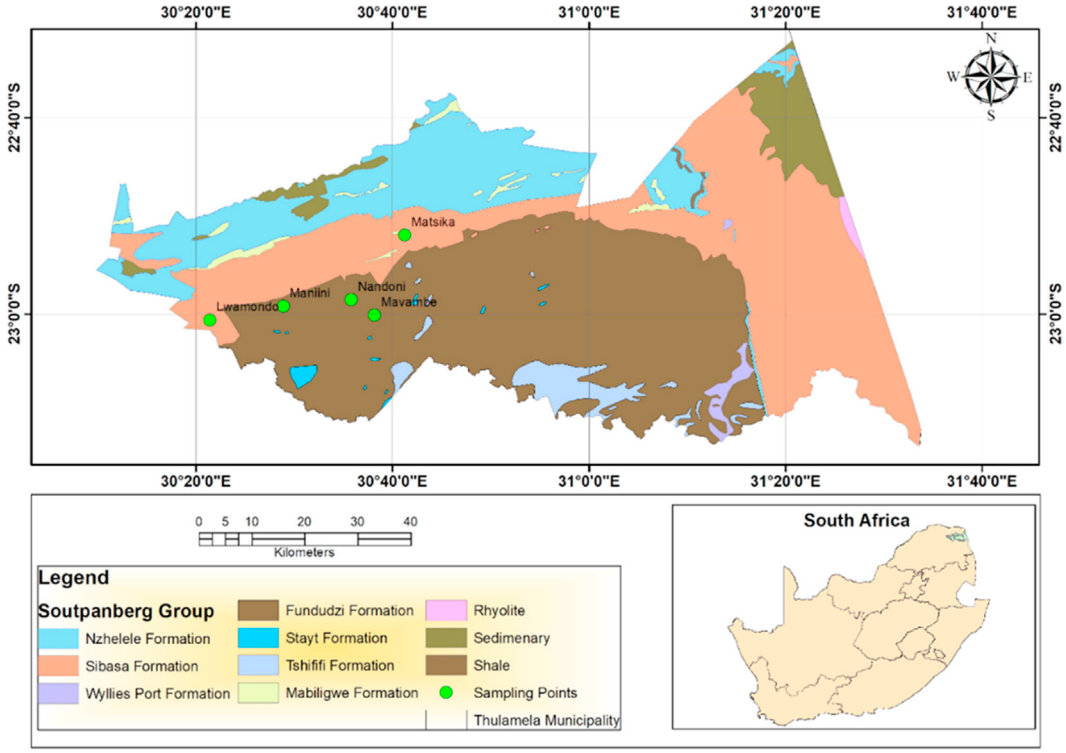

Figure 1. Distribution of clayey deposits in the study area.

Whilst the receiving slit was positioned at 0.040°, counting area was from 5 to 70° on a 2θ scale at 1.5s. The clay phases were identified using X'PertHighscore plus software (Omotoso et al., 2006). For details, the mentioned study provides information on Rietveld refinement (Autoquan Program) which was employed to compute the relative phase amounts of the mineral components (w%).

3.3. Geochemical analysis

Major and trace element geochemical analyses of the fine bulk clay were quantitatively estimated using PANaytical AXios X-Ray fluorescence (XRF) spectrometer at the University of Venda, Limpopo, South Africa. The clay samples were pulverized to obtain <32 μm fractions and then calcined at 1000 °C for minimum period of three hours in order to oxidize iron (ii) oxide (Fe^{2+}) and sulphur (S). Pressed powder pellets for XRF analyses were prepared using 6 g of sample powder and 12 g of boric acid as a binder. The mixture was fused into a steel cup and pressed at a pressure of 30 tons in hydraulic set (Reimold et al., 1994). The XRF instrument equipped with a 4 kW Rhodium (Rh) tube was used to analyze major oxides by inserting a glass disks containing 1 g calcined sample, 8 g flux composed of 35% alkali borate ($LiBO_2$) and 64.71% lithium tetra borate ($Li_2B_4O_7$) as oxidant at 1050 °C into the XRF equipment. For details, the work of Reimold et al. (1994) describes the accuracy, precisions, procedures and standards employed for this analysis.

3.4. Thermal stability analysis

The thermal analysis was conducted to determine the thermal stability of samples and to provide information regarding mass changes in mineralogy of the clay samples as the temperature increases at the Stellenbosch University in South Africa. The differential thermal (DTA) was conducted using Setaram apparatus which was calcined with inert substance (Al_2O_3). Samples were obtained based on principles of stokes law of sedimentation of clay and placed in sample holder of the furnace. The sample holder was a piped block with two small holes for the sample and inert substance. Differential thermocouple junction wire was inserted into the sample and inert substance holder while the heat source was powered. The maximum temperature attained was 1000 °C at a heat rate of 25 °C/min for 5 h owing to the heat capacity which the inert substance can withstand. The temperature difference between sample and calcined inert substance (Al_2O_3) was recorded after undergoing identical thermal cycles. The differential temperature was then plotted against time as DTA curve. The degree of structural stability was evaluated from both the dehydroxylation temperature and asymmetry of the endothermic peak. Slope ratio was also obtained by calculating the ratio of the limiting gradients of the exothermic and endothermic material in a liquid medium.

3.5. Microstructural test

Micro structural pores and topography of the studied clays were determined using a Ziess EVO MA15 scanning electron microscope (SEM) equipped with a tungsten filament. A Bruker energy dispersive X-ray spectrometer was used for the morphological analysis. The system was operated under high vacuum of approximately 2.15 e-006 mbars. The electron beam was generated with an accelerating voltage of 20 KV and probe current of approximately 2 nA. The clay sample was sprinkled onto a carbon tape substrate and carbon coated prior to being loaded into the SEM. A secondary electron detector was used to produce images at 300X, 600X and 900X magnifications. Some of these particles are out of focus owing to the three-dimensional depth loss of information. Focusing on one part results in the other being out of focus on some of the images particularly at the high magnification.

3.6. Physical tests

3.6.1. Particle size distribution

The grain size analysis was conducted when collected samples were first air-dried until constant mass was achieved and 500 g of weighed soil samples were shaken through a stack of sieves with openings of decreasing size from top to bottom using mechanical shaker. The mass of soil retained and passing each sieve was weighed and recorded after the soil was shaken on mechanical shaker. The percent finer on each sieve size was determined using Eq. (1). 50 g of soil which passed through No 200 sieve or <75 μm fractions were treated with hydrogen peroxide (H_2O_2) solution in order to oxidize organic material. The resultant slurry is mixed with 125 ml of 4% sodium hexametaphosphate ($NaPO_3$) solution which act as the deflocculating agent. The sedimentation was based on the principle of stroke's law in which particles fall freely at steady velocity under the gravity influence (Nyakairu et al., 2002).

$$F = \frac{\sum M - (M_1 + M_2 + \ldots M_i)}{\sum M} \quad (1)$$

where $\sum M$ is the summation of the cumulative mass retained in each sieve, $\sum M - (M_1 + M_2 + \ldots M_i)$ is the cumulative mass of soil retained above each sieve, and F is the percent finer on each sieve size.

3.6.2. Atterberg test, pH and colour

The degree of plasticity of studied samples was achieved through determination of Atterberg's liquid (LL) and plastic limit (PL) using Casagrande apparatus (Casangrande, 1947) in accordance with the ASTM-D4318 standard. Prior to commencement of the procedure for liquid limit the apparatus was properly adjusted to the consistency height of 10 mm. Correctness of calibration was confirmed by vibrated sound when the crank struck the cam follower. Subsequent trials were repeated producing successive number of blows to close the grooves. The number of blows (N), as the ordinates on the logarithmic scale, was plotted against the moisture contents as the abscissae on the arithmetic scale using semi-logarithmic graph paper. The flow curve was a straight line of best-fit drawn as nearly as possible through the plotted points to determine the moisture content at 25 blows.

To determine the pH of the soil about 100 ml of de-ionized water was added to 100 g of pulverized clay samples placed in a 100 ml beaker. The clay solution was stirred continuously for an hour using stirring rod until a homogeneous solution was achieved. This was to allow the pH of the soil slurry to stabilized. The pH meter was calibrated with buffer solutions of pH 4.00 and 7.00 to standardize the acid-base condition. The thermometer was used to measure the temperature after which the pH meter electrodes were inserted into the soil slurry. After two minutes, the displayed value was read and recorded.

The colours of raw clayey material were determined using the Munsell colour chart. The chart consists of standard colours in different hue, value and chroma. The colour of clayey sample on the white sheet was compared and correlated with the standard colour of Munsell chart to determine its hues, value and chroma. The colour test provides information about colour stability and mineral composition of clays when subjected to engineering and mineralogical tests.

3.6.3. Cation exchange capacity (CEC)

The CEC of clay sample was determined using exchangeable cation extraction and atomic absorption spectrometer. About 25 g of the sample was initially oven dried at 110 °C for six hours until constant weight was achieved. The sample pH was later adjusted to near-neutral when diluted with 1 L of NH_4OH inside a 500 mL conical flask. The near-neutral solution was then thoroughly mixed with 125 mL of 1M NH_4O_{AC} for 12 h using a mechanical shaker. With the aid of suction machine, the solution was poured into a funnel lined with filter paper. The filtrate was re-filtered until the solution is clear by pouring 25 mL of 1M NH_4O_{AC} into the suction clay solution. The cleared filtrate was then poured into a

beaker for determination of exchangeable cation such as Na^{+}, K^{+}, Ca^{2+} and Mg^{2+} using atomic absorption spectrometer. The results of detected cations were displayed on the computer screen connected to the spectrometer and given in ml/g although converted to meq/100 g using Eqs. (2), (3), 4 and, (5) (Chapman, 1965)

$$\text{Total solution (ml)} = \text{final tube weight (g)} - \text{tube tare weight (g)} - 2\text{g(weight of soil used)} \quad (2)$$

$$\text{Mg in solution, not on CEC (meq)} = \text{Total solution(mls)} \times 0.003\text{(1.5mM MgSO4 has 0.003meq.l} \quad (3)$$

$$\text{Total Mg added (meq)} = 0.1\text{meq(meq in 10mls of 5mM MgSO4)} + \text{meq added in 0.1M MgSO4} \quad (4)$$

$$CEC(meq/100g) = (c - b) \times 50(\text{total Mg added} - \text{Mg in final solution}) \quad (5)$$

3.7. Mechanical tests

The compressive strength of the bricks was tested at loading rate of 140 kg/cm^2/min following international procedures ASTM C67-03 from which the national standard SANS227:2007 was adopted. Three representative brick specimen which cover texture, colour and sizes were subjected to vertical load force until failure thus recorded as strength. The external dimensions of each sampled brick were measured and marked for identification with the weight recorded in grams.

The water absorption test of the bricks was conducted to determine the durability and suitability of the bricks for building purposes using the ASTM C67-17. This was carried out by soaking the bricks in water for a period of 24 h. A total of 20 burnt bricks were used to carry out the test. The bricks were first weighed dry and this was recorded as weight 1 (w1), then they were soaked in cold water for 24 h and were weighed again after soaking, the weight after soaking was recorded as weight 2 (w2). The percentage of the water absorbed was then calculated. The water absorbed by the brick was indicated by the difference in w2 and w1. The water absorption value for each site was indicated by the average values of the brick replicates for each location.

4. Results and discussion

4.1. Mineral composition characterization

The results of the mineralogical analysis of studied clayey material are presented in Table 1 while Figure 2 shows the XRD diffractogram patterns. The result mainly depict the presence of kaolinite and chlorite minerals while the non-clay minerals included quartz, feldspar, talc and Hornblende. In most samples, Kaolinite content ranged from 22.80% to 59.26% when sample from L1 was found to have highest value. The kaolinite mineral was found as a main clay mineral in samples from L1 (59.26%) and L3 (25.19%) whose values were comparatively higher than L5 (22.80%) although absent in chlorite content. Chlorite were found present in all samples except in L1 and L3 samples while clays from L5 and L2 have higher values of 9.07% and 8.83% respectively. The presence of kaolinite and chlorite as the major clay mineral suggest the

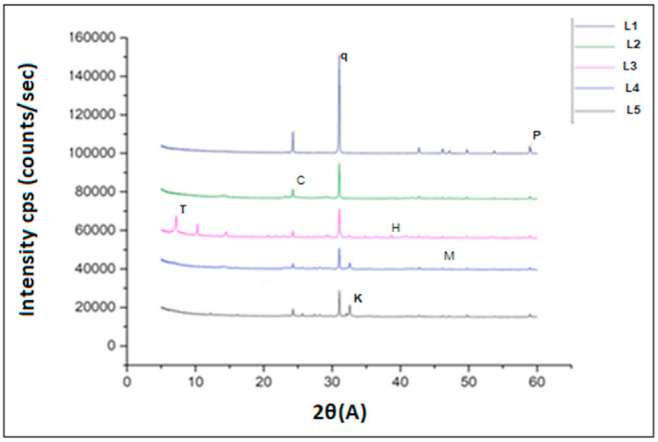

Figure 2. X-ray diffractograms patterns of the studied clayey material (Note: Q-quartz; P-plagioclase; K-kaolin; C-chlorite; H-hornblende, M-microline, T-talc).

weathering product of feldspar and mafic silicate. This explains the presence of plagioclase and hornblende which are mafic-rich silicate minerals. The absence of smectite proposes low potential of cracking during drying or firing (Dacosta et al., 2013) whilst Illite has been reported to provide auspicious properties for ceramic use (Bennour et al., 2015; Mahmoudi et al., 2016). Although talc, hornblende and chlorite are relatively low, their presence connote metamorphic provenance of the clayey raw material.

4.2. Geochemical compositions characterization

The geochemical result for the studied clay show the presence of major element such as Si, Al, Na, K, Mg, Ca, Ti, Fe and Mn in their oxide forms. The result show varying amount of silica (34.1–59.5%), alumina (14.30–22.4%), sodium oxide (0.1–1.3%), potassium oxide (0.3–3.0%), magnesia (0.1–1.3%) and calcium oxide (0.1–1.7%) in studied bulk clays. The fluxing oxides of the samples namely K_2O, N_2O, CaO, MgO, MnO and P_2O_5 are generally low in content with average abundance ranging from 0.06% to 1.78% (Table 2). The low content of the fluxing oxides consequently reduces the mullites and crystobalites phases formation during vitrification as temperature increases hence lower density or strength of clayey product (Diko et al., 2011). The iron oxide content, Fe_2O_3, varies (4.8–25.5%) thus reflects heterogenous stability in tonality and colour. The result of the Musell colour test shows redox reaction of the iron content in terms of strong brown, red, brown and yellow red colours displayed. The manganese oxide (MnO) may have contributed to the varied colour as well despite its relatively low content (Darweesh et al., 2012). Most of the studied samples have relatively high Al_2O_3 content which suggest the bauxitic composition from which kaolinite minerals might have ensued.

4.3. Thermal description of clayey material

The results of the differential thermal (DTA) for the studied clayey materials are presented in Figure 3. There are two conspicuous endothermic and exothermic peaks which characterizes studied clayey materials. The endothermic reaction occurred at 200 °C and 610 °C while

Table 1. Mineralogical analysis of the raw clayey material.

Location		Kaolinite	Chlorite	Quartz	Plagioclase	Microcline	Hornblende	Talc
Lwa	L1	59.26	-	22.61	38.16	-	9.23	-
Nan	L2	-	8.83	37.39	-	16.35	4.34	-
Mat	L3	25.19	-	59.87	33.09	-	1.95	13.35
Mav	L4	-	8.03	42.02	-	7.53	4.26	-
Man	L5	22.80	9.07	34.88	24.82	4.66	-	5.79

Table 2. Chemical analysis of the studied clayey material.

Location	SiO_2 (%)	Al_2O_3 (%)	Fe_2O_3 (%)	MnO (%)	MgO (%)	CaO (%)	Na_2O (%)	K_2O (%)	CIA	k/Cs	SiO_2/Al_2O_3	lol
Lwa	34.1	22.4	25.5	0.2	0.1	0.1	0.1	0.5	97.7	851.9	1.5	15.2
Nan	59.5	16.0	4.8	0.1	1.3	1.2	1.3	3.0	95.7	1111.1	2.4	10.9
Mat	48.3	20.10	14.6	0.1	0.4	0.3	0.1	0.3	77.0	2963.0	3.8	12,4
Mav	54.1	14.30	5.9	0.1	1.2	1.7	0.9	1.6	74.1	5629.6	3.7	17.7
Man	47.0	19.50	9.8	0.1	0.8	1.3	0.1	1.3	87.8	2351.9	2.4	17.5

the exothermic event conspicuously peaked at 100 °C and 450 °C. The first endothermic reaction was attributable to the expulsion of weakly bond and adsorbed water which corresponds to mass loss of about 1.2% as indicated by the temperature curve. The second endothermic reaction occurred at temperature range from 500 °C to 650 °C. Similarly, the first exothermic expansion was noted near 100 °C due to expulsion of surface water from the samples while the second exothermic peak occurred near 450 °C. The temperature corresponds to decomposition of organic matters. At this temperature where the total mass loss was 3.8%, polymorphic transformation of α-quartz to β-quartz is suggested to have occurred as observed by dehydroxylation reaction. At exothermic reaction trend near 900 °C, a total mass loss of 6.6% (L5), 7.2% (L1), 8.4% (L3), 6.2% (L2) and 2% (L4) which correspond to complete destruction of the clay minerals and decarbonacious reaction were observed and thus consistent with the work of Boussen et al. (2016) As temperature rise above 900 °C, the clayey materials show progressive increase until 1000 °C while samples from Manini at 800 °C. This temperature suggests that the threshold of new crystallization processes has been reached. It was indicated that new mineral such spinel is usually accompanied by rapid shrinkage during the process (Mahmoudi et al., 2017; Zhang et al., 2017).

4.4. Microstructural and pore characterization

The scanning electron (SEM) photomicrographs of all the studied samples are presented in Figure 4. The surface topography of all studied samples varies from coarse to fine texture although replete with macropores of >50 nm. Variation in the shapes from spherical to irregular dimensions can be adduced to different particle sizes present in samples whilst the coarse topography suggests the presence of resistant minerals, such quartz, to weathering. The fine texture indicates the mineral that are susceptible to weathering such plagioclase and microcline. The platy shaped orientation indicates that atomic arrangement in the layered structure of clayey minerals glides each other hence imparts plasticity properties. Tiny pore and stroma were present in all samples although with pore sizes >50 nm. The pore volume constituted a capillary system in which molten minerals such as mullite, spinel and crystobalites that usually formed at higher temperature can saturate.

4.5. Physical tests

4.5.1. Particle size distribution

The particle size of the studied samples averagely consist of 90% of sand fractions, 6% of silt fractions and 4% of clay fractions (Table 3) and the engineering properties such as the coefficient of uniformity (C_u), coefficient of gradation (C_c) were determined (Zhang et al., 2017). Based on the textural properties, the studied samples are designated as elastic silt (MH), lean clay (CL), inorganic silt (ML) soils under the Unified Soil Classification System (USCS). All samples showed homogeneous distribution of sand size fractions (2–0.05 mm) with compositional values ranging from 86.98-98.66% and the gradational curve followed a decreasing order from L4> L2 > L3 > L5> L1 samples (Figure 5). Similarly, the clay fines fraction with size diameter ranging from 2 μm to 0.05 mm showed heterogeneous abundance with average value greater 10% particularly in L1 sample. This may be attributed to relatively higher content of Al_2O_3 from which more kaolinite could have weathered as revealed in the XRF and XRD results. Holistically, the gradational estimation depicted that all the soils collected from L1, L5, L4 and L3 showed a well sorted and graded pattern with exception of soils from L2 location.

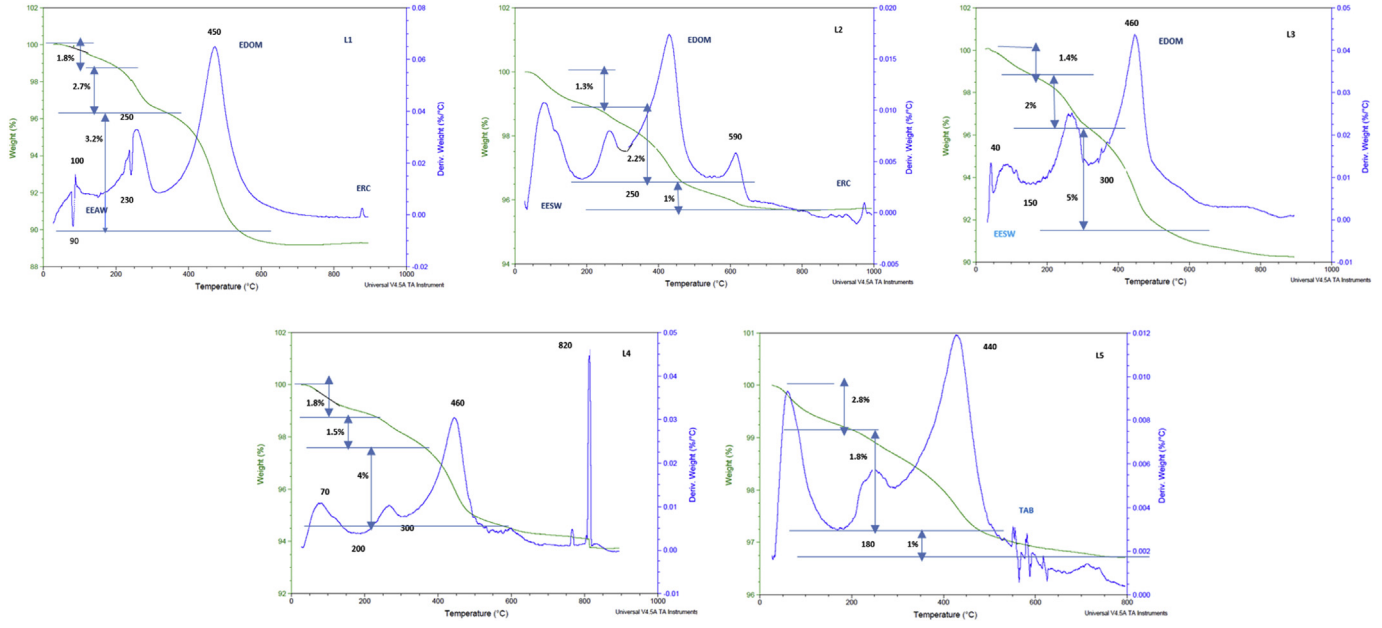

Figure 3. Thermogravimetry curves of the studied samples showing EESW-endothermic expulsion of surface water, EEAW-Endothermic expulsion of absorbed water, EEWA- Exothermic expulsion of weakly bond water, EDOM-Endothermic decomposition of organic matters, TAB-polymorphic transformation of α-quartz to β-quartz, ERC-Exothermic recrystallization reaction in L1 to L5.

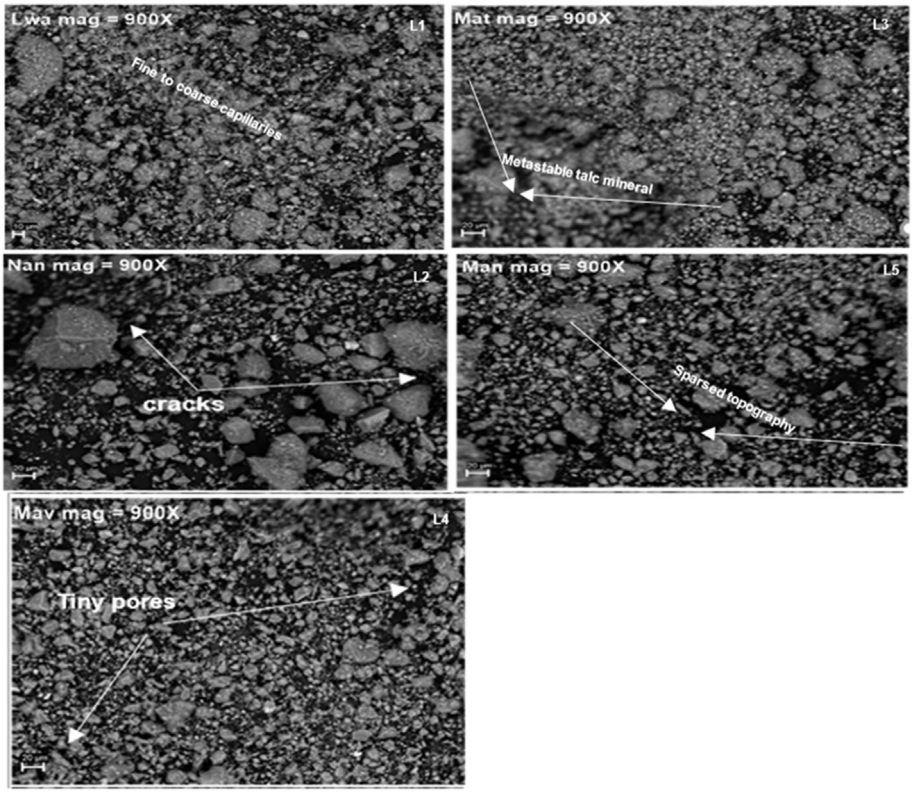

Figure 4. Scanning Electron Microscope (SEM) Photomicrographs showing L1- fine to coarse capillary systems, L2- crackly capillary system, L3- dissolved mineral capillary system, L4- extensional capillary system, L5- pores capillary system.

Table 3. Textural properties of studied soil samples.

Location	Grain sizes composition (%)			Engineering parameters							
	Sand	Silt	Clay	D_{10}	D_{30}	D_{60}	D_{75}	C_u	C_c	S_o	USCS
L1	94.39	3.43	2.21	0.07	0.22	0.55	0.80	7.86	1.26	2.11	MH
L2	98.56	0.80	0.62	0.06	0.15	0.35	0.50	6.36	1.17	2.04	ML
L3	96.41	1.99	1.68	0.12	0.25	0.70	1.50	5.83	0.74	2.67	ML
L4	98.66	0.78	0.62	0.15	0.35	0.75	1.00	5.00	1.09	1.83	CL
L5	96.67	1.94	1.36	0.12	0.28	0.62	0.88	5.17	1.05	2.00	CL

Note: MH-Elastic silt; CL-Lean clay; ML-inorganic silt.

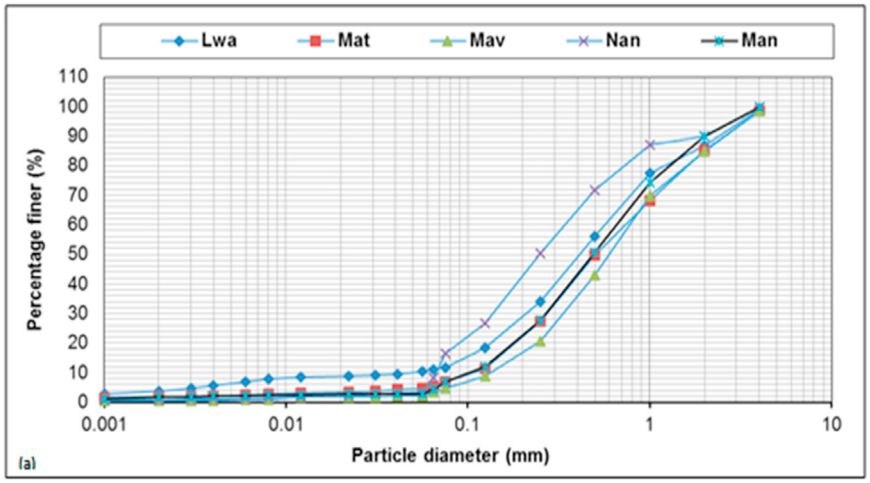

Figure 5. Particle size distribution of the studied samples.

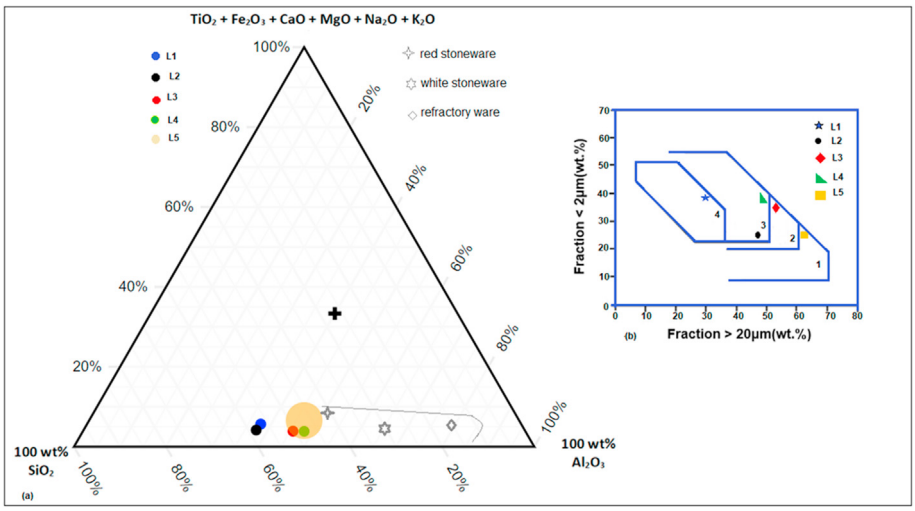

Figure 6. (a) Riley's plot showing possible clay utilization (b) Winkler's chart showing potential use of clay for (1) common bricks, (2) vertically perforated bricks, (3) roofing tiles and masonry bricks (4) hollow products.

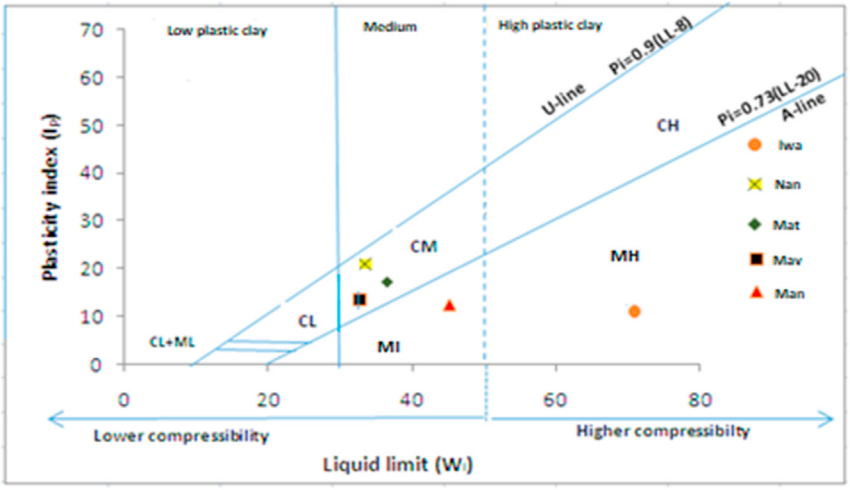

Figure 7. Plasticity chart showing degree of compressibility of studied clays.

Table 4. Summary of physical properties of studied clay samples.

Location		Hue/value/chroma	Colour	Soil pH	CEC (Meq/100 g)
Lwa	L1	5YR/5/8	Yellowish red	6.13	20.69
Nan	L2	7.5YR/5/4	brown	7.02	17.60
Mat	L3	7.5YR/4/6	Strong brown	6.99	27.86
Mav	L4	7.5YR/5/8	Strong brown	7.5	37.05
Man	L5	2.5YR/5/8	Red	6.78	42.73

This could be due to the presence of relative higher abundance of sand size fractions and lowest fines sizes compared to others. According to Winkler's diagram the grain size distribution shows that the samples from location 2 and 4 are suitable for roofing tiles and masonry bricks while samples from location 1, 3 and 5 could be used for common bricks, vertically perforated bricks and hollow products respectively (Figure 6b). In addition, the studied samples show possible uses for red stonewares and while stoneware (Fiori et al., 1989).

4.5.2. Atterberg limits, pH

The plasticity properties of the clay deposits exhibited heterogeneous behaviors as revealed in plastic limit (PL), liquid limit (LL) and plastic index (PI) values presented Figure 7. This A-line separated the inorganic clay above the line from the inorganic silts below the line. Thus, the L1 samples indicate inorganic silts of high compressibility and organic clays properties due to their position below the A-line in plasticity chart. The studied samples from locations L2, L4 and L5 were found to be having LL values that are greater than 50 but lower PI value than 30 when compare with clayey samples from L1 location. This indicated that these soils are inorganic silts with high compressibility and organic clays properties since it plotted below the A-line of plasticity chart. The samples from L3 location were found to be having medium plasticity properties with LL values ranging from 30 to 50 and plotted below the A-line of plasticity chart where intermediate PI value ranged from 15 to 21. According to the Unified Soil Classification System, soils from L1 are considered as elastic

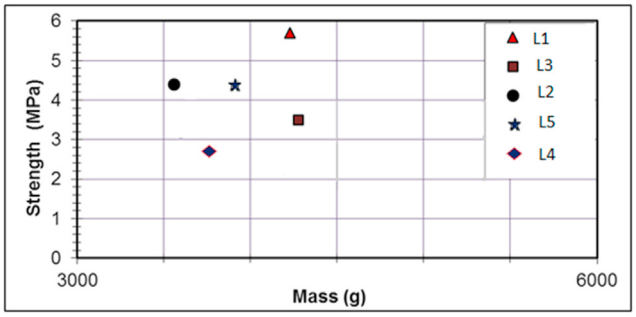

Figure 8. Compressive strength of bricks against their masses.

silt (MH) due to their coefficient of uniformity (C_u) < 3 and have >50% liquid limit values which plotted above the "A" line (See Figure 5). Furthermore, soils from L5 which plotted below the "A" line are considered as inorganic silt (ML) while those from L2, L3 and L4 are regarded as clayey sand.

The raw clays varied in hue/value/chroma with their corresponding tonality shades (Table 4). Their hue/value/chroma ranged from 2.5YR/5/8 to 10YR/5/1 with corresponding tonality of red and gray. The clayey material that exhibits pale yellow to gray colour suggests reducing properties of the soil due to leachable Fe resulting from hydromorphic conditions. The reddish to very pale brown sample indicates that oxidizing nature where Fe was enriched during their formation processes. Clay samples of L1 and L5 whose Fe content is relatively high (above 5%) exhibited a deep tonality. The CEC values of studied samples widely varied from 17.60 to 42.73 meq/100 g and soil pH exhibited similar near-neutral-pH values ranging from 6.13 to 7.50. Samples from L5 and L4 have relatively high CEC values above 30 meq/100 g compared to other samples in which their CEC values are below 30 meq/100 g. Studied samples with CEC value above 30 meq/100 g may likely experience efflorescence effect owing to Ca^{2+} ion which could adhere to the surface area of the clayey material although insignificance amount of Ca oxide was found in all studied samples. Some previous studies (Riaz et al., 2019; Saidian et al., 2016; De Jonge et al., 1996) have provided plausible arguments that the CEC properties highly correlates to the adsorption specific surface of any clayey material at neutral or near neutral pH.

4.6. Mechanical tests

4.6.1. Compressive strength

Figure 8 shows the results of the average compressive strength test of the bricks against the mass. The average strength value range from 2.9 to 5.2 MPa in which brick specimens from L1 and L4 have highest and lowest crushing strength value respectively. In comparison to brick specimens from L2 with 3.8 MPa strength value, the L3 and L5 bricks showed relatively higher of 4.3 and 4.1 respectively. Bricks specimens from L1, L3 and L5 have relatively higher compressive strength values than L2 and L4 possibly because of higher content of kaolinites whose pores are not effectively connected hence denser with high thermal stability. On the other hand, specimens from L2 and L4 are dominated with chlorite whose open pores are relatively larger on the surface hence lower density and compressive strength. The ASTM C67-03 and SANS227:2007 standards stipulate the average compressive strength values of 4.0 MPa for on-site manufacture, 5.0 MPa for off-site manufacture and 10 MPa for double storey constructions. Based on the individual and average compressive strength values obtained, the bricks from L1, L3 and L5 are suitable for on-site single storey construction because values are above 3.2 and 4.0 MPa respectively while L2 and L4 do not meet the standards. However, none of the studied brick specimen has crushing strength suitable for off-site double storey constructions

Table 5. The water absorption of the bricks.

Sample number	Initial weight of dry bricks W1 (kg)	Final weight of bricks W2 (kg)	Water absorption $\frac{w2-w1}{w1} \times 100$	Average % water absorption
L1	2.509	2.813	10.806	11.01
	2.412	2.725	11.486	
	2.624	2.945	10.899	
	2.463	2.802	12.098	
	2.532	2.807	9.796	
L2	3.140	3.643	13.807	14.65
	3.040	3.567	14.774	
	3.335	3.911	14.727	
	3.098	3.644	14.984	
	2.896	3.406	14.974	
L3	2.619	2.993	12.496	11.88
	2.562	2.905	11.807	
	2.526	2.854	11.493	
	2.516	-	-	
	2.713	3.074	11.744	
L4	3.214	3.901	17.610	18.15
	3.147	3.877	18.828	
	3.101	3.892	20.323	
	3.261	3.911	16.619	
	3.167	3.833	17.375	
L5	3.762	4.332	13.158	13.00
	3.993	4.551	12.261	
	3.479	3.988	12.763	
	3.432	3.963	13.399	
	3.964	4.580	13.449	

Note: "- "indicates the brick dissolved in water.

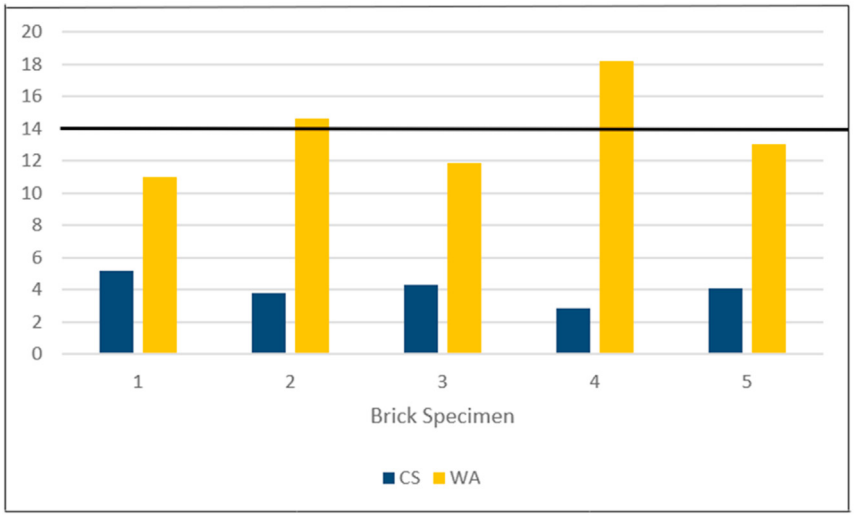

Figure 9. Relationship between water absorption (WA) and compressive strength (CS).

because their individual and average values are below 8 MPa and 10 MPa. This reveals that the dominant kaolinite minerals have minimal effect on strength formation while the iron oxides enhance the cementation as depicted in the compressive strength results.

4.6.2. Water absorption

The results of water absorption (WA) tests conducted on twenty brick specimen from different locations in the study are presented in Table 5. It reveals average water absorption values of 11.01%, 14.65%, 11.88%, 18.15% and 13.00% for locations L1, L2, L3, L4 and L5 respectively. Brick specimen from location L1, L3 and L5 have WA values less than 14% which suggests their suitability for engineering construction according to SANS 227:2007 and ASTM standards while brick from L2 and L4 are unsuitable due to higher values above the required standard. This indicate suggests that the pore volume and capillarity for L2 and L4 bricks are comparatively highly than other bricks hence absorbing more water molecules. Although the average WA value for L3 meets the required standard, some brick specimen completely dissolved in water within a 24-period. This could be attributed to higher content of talc in their composition which expands to dissolve when mixed with water or under-firing of brick during manufacturing process. The suitability of brick for engineering purpose in terms of WA was found to correlate with compressive strength as shown in Figure 9.

5. Conclusions

The studied clayey raw materials are found to be composed mainly of kaolinites and chlorite clay minerals besides other non-clay minerals such iron oxide, quartz and plagioclase. Majority of the studied raw materials demonstrate their suitability for single-storey construction bricks based on their mechanical and durability tests compliance with SANS and ASTM standards. Based on the parameter characterization, the chlorite-rich clayey raw material may be unsuitable for light weight masonry burnt brick compared to kaolinite rich clayey materials because they showed higher compressive strength and low water absorption properties.

Declarations

Author contribution statement

G. O. Akintola: Conceived and designed the experiments; Performed the experiments; Analyzed and interpreted the data; Contributed reagents, materials, analysis tools or data.

F. Amponsah-Dacosta: Analyzed and interpreted the data; Contributed reagents, materials, analysis tools or data.

S. E. Mhlongo: Performed the experiments; Analyzed and interpreted the data; Contributed reagents, materials, analysis tools or data.

Funding statement

This work was supported by The University of Venda, South Africa.

Declaration of interests statement

The authors declare no conflict of interest.

Additional information

No additional information is available for this paper.

Acknowledgements

The authors are grateful to Humbulani Thavhanyedza who helped with plotting of maps and other spatial diagrams. We appreciate SGS, Mintek and University of Pretoria for assisting with laboratory characterizations. Finally, we acknowledge the anonymous reviewers and editorial teams for their helpful comments which have greatly improved this work.

References

Anhaeusser, 2006. Ultramafic and mafic intrusions of the kaapvaal craton. In: Johnsonn, M.R., Anhaeusser, C.R., Thomas, R.J. (Eds.), The Geology of South Africa', pp. 95–134.

Amponsah-Dacosta, Francis, Muzerengi, Confidence, Mhlongo, Sphiwe Emmanuel, Mukwevho, Gudani F., 2013. Characterization of clays for making ceramic pots and water filters at mukondeni village, limpopo province, South Africa. J. Eng. Appl. Sci. 8, 927–932.

Barker, O.B., Brandl, G., Callaghan, C.C., Eriksson, P.G., Van Der Neut, M., 2006. The soutpansberg and waterberg groups and the blouberg formation. Geol. South Afr. 301–318.

Bennour, A., Mahmoudi, S., Srasra, E., Hatira, N., Boussen, S., Ouaja, M., Zargouni, F., 2015. Identification and traditional ceramic application of clays from the chouamekh region in south-eastern Tunisia. Appl. Clay Sci. 118, 212–220.

Bordy, Emese M., Catuneanu, Octavian, 2002. Sedimentology and palaeontology of upper karoo aeolian strata (early jurassic) in the tuli basin, South Africa. J. Afr. Earth Sci. 35, 301–314.

Boussen, Sghaier, Chaabani, Jamoussi, Bennour, 2016. Characteristics and industrial application of the lower cretaceous clay deposits (bouhedma formation), southeast Tunisia: potential use for the manufacturing of ceramic tiles and bricks. Appl. Clay Sci. 123, 210–221.

Chapman, H.D., 1965. Cation-exchange capacity. Methods Soil Anal.: Part 2 Chem. Microbiol. Propert. 9, 891–901.
Darweesh, H.H.M., Wahsh, M.M.S., Negim, E.M., 2012. Densification and thermomechanical properties of conventional ceramic composites containing two different industrial byproducts. Am.-Eurasian J. Sci. Res. 7, 123–130.
Petersen, L.W., Moldrup, P., Jacobsen, O.H., Rolston, D.E., 1996. Relations between specific surface area and soil physical and chemical properties. Soil Sci. 161 (1), 9–21.
Diko, M.L., Ekosse, G.E., Ayonghe, S.N., Ntasin, E.B., 2011. Physical characterization of clayey materials from tertiary volcanic cones in limbe (Cameroon) for ceramic applications. Appl. Clay Sci. 51, 380–384.
Ekosse, Georges E., 2010. Kaolin deposits and occurrences in africa: geology, mineralogy and utilization. Appl. Clay Sci. 50, 212–236.
El Idrissi, Daoudi, El Ouahabi, Collin, Fagel, 2018. The influence of clay composition and lithology on the industrial potential of earthenware. Construct. Build. Mater. 172, 650–659.
Fadil-Djenabou, Ndjigui, Mbey, 2015. Mineralogical and physicochemical characterization of ngaye alluvial clays (northern Cameroon) and assessment of its suitability in ceramic production. J. Asian Ceram. Soc. 3, 50–58.
Fiori, Fabbri, Donati, Venturi, 1989. Mineralogical composition of the clay bodies used in the Italian tile industry. Appl. Clay Sci. 4, 461–473.
Hajjaji, Kacim, Boulmane, 2002. Mineralogy and firing characteristics of a clay from the valley of ourika (Morocco). Appl. Clay Sci. 21, 203–212.
Jung, Yoo, Lee, Park, Lee, Kim, 2019. Clay mineralogical characteristics of sediments deposited during the late quaternary in the larsen ice shelf b embayment, Antarctica. Minerals 9, 153.
Kröner, Jaeckel, Brandl, Nemchin, Pidgeon, 1999. Single zircon ages for granitoid gneisses in the central zone of the limpopo belt, Southern Africa and geodynamic significance. Precambrian Res. 93, 299–337.
Kröner, Jaeckel, Brandl, 2000. Single zircon ages for felsic to intermediate rocks from the pietersburg and giyani greenstone belts and bordering granitoid orthogneisses, northern kaapvaal craton, South Africa. J. Afr. Earth Sci. 30, 773–793.
Lahcen, Hicham, Latifa, Abderrahmane, Jamal, Mohamed, Meriam, Nathalie, 2014. Characteristics and ceramic properties of clayey materials from amezmiz region (western high atlas, Morocco). Appl. Clay Sci. 102, 139–147.
Loutou, Taha, Benzaazoua, Daafi, Hakkou, 2019. Valorization of clay by-product from moroccan phosphate mines for the production of fired bricks. J. Clean. Prod. 229, 169–179.
Mahmoudi, Bennour, Meguebli, Srasra, Zargouni, 2016. Characterization and traditional ceramic application of clays from the douiret region in south Tunisia. Appl. Clay Sci. 127, 78–87.
Mahmoudi, Bennour, Srasra, Zargouni, 2017. Characterization, firing behavior and ceramic application of clays from the gabes region in south Tunisia. Appl. Clay Sci. 135, 215–225.
Mahmoudi, Srasra, Zargouni, 2008. The use of tunisian barremian clay in the traditional ceramic industry: optimization of ceramic properties. Appl. Clay Sci. 42, 125–129.
Manoharan, Sutharsan, Dhanapandian, Venkatachalapathy, 2012. Characteristics of some clay materials from tamilnadu, India, and their possible ceramic uses. Cerâmica 58, 412–418.
Murray, 2000. Traditional and new applications for kaolin, smectite, and palygorskite: a general overview. Appl. Clay Sci. 17, 207–221.
Ntouala, Onana, Kamgang, Ekodeck, 2016. Mineralogical, geochemical and mechanical characterization of the ayos (east-Cameroon) lateritic and alluvial clayey mixtures: suitability for building application. J. Build. Eng. 5, 50–56.
Nyakairu, Kurzweil, Koeberl, 2002. Mineralogical, geochemical, and sedimentological characteristics of clay deposits from central Uganda and their applications. J. Afr. Earth Sci. 35, 123–134.
Obaje, Omada, Dambatta, 2013. Clays and their industrial applications: synoptic review. Int. J. Sci. Technol. 3, 264–270.
Omotoso, Mccarty, Hillier, Kleeberg, 2006. Some successful approaches to quantitative mineral analysis as revealed by the 3rd Reynolds cup contest. Clay Clay Miner. 54, 748–760.
Refaey, Jansen, El-Shater, El-Haddad, Kalbitz, 2015. Clay minerals of pliocene deposits and their potential use for the purification of polluted wastewater in the sohag area, Egypt. Geoderma Reg. 5, 215–225.
Reimold, Koeberl, Bishop, 1994. Roter kamm impact crater, Namibia: Geochemistry of basement rocks and breccias. Geochem. Cosmochim. Acta 58, 2689–2710.
Riaz, Khitab, Ahmed, 2019. Evaluation of sustainable clay bricks incorporating brick kiln dust. J. Build. Eng. 24, 100725.
Saidian, Godinez, J., Prasad, 2016. Effect of clay and organic matter on nitrogen adsorption specific surface area and cation exchange capacity in shales (mudrocks). J. Nat. Gas Sci. Eng. 33.
Seong, 2005. Sustainable Mining of the clay Resources in Peninsular malaysia.
Xie, Kröner, Brandl, Wan, 2017. Two orogenic events separated by 2.6 ga mafic dykes in the central zone, limpopo belt, southern africa. Precambrian Res. 289, 129–141.
Yongue-Fouateu, Ndimukong, Njoya, Kunyukubundo, Mbih, 2016. The ndop plain clayey materials (bamenda area – nw Cameroon): mineralogical, geochemical, physical characteristics and properties of their fired products. J. Asian Ceram. Soc. 4, 299–308.
Zhang, Kong, Yin, Chen, 2017. Engineering geology of basaltic residual soil in leiqiong, southern China. Eng. Geol. 220, 196–207.